Semicond. Sci. Technol. 8 (1993) 1291–1297. Printed in the UK

Simulation of electron transport in silicon: impact-ionization processes

M J Martín, T González, J E Velázquez and D Pardo

Departamento de Física Aplicada, Facultad de Ciencias, Universidad de Salamanca, 37008 Salamanca, Spain

Received 16 December 1992, in final form 18 March 1993, accepted for publication 5 April 1993

Abstract. Using non-parabolic ellipsoidal X and L valleys to represent the conduction band of Si, we have developed a Monte Carlo simulation for the study of electron transport properties in this material, under both low and high electric field conditions. Employing a simple model for the characterization of the impact ionization processes we have obtained the ionization coefficient and the probability of electron ionization. The results highlight the importance of the L valleys in very high transport phenomena, and compare favourably with other experimental and theoretical data.

1. Introduction

Impact ionization in semiconductors is a basic process in the functioning of certain devices such as photodetectors, and also occurs in others (MOSFETs) when operating at high electric fields, being an important source of device degradation. These ionization processes occur at very high fields, such that the carriers that cause them must be very energetic. In an attempt to explain these carrier generation phenomena it is necessary to take into account certain high-energy valleys in which they may take place. In the particular case of Si it is necessary to use a conduction band formed of X and L valleys to study the impact ionization processes of electrons, as has been suggested by other authors [1–3].

Assigning an analytical expression to the X and L valleys of the Si conduction band and proposing a simple model for the impact ionization processes, the present work aims to perform a characterization of electron transport in Si that yields good results both at low electric fields (average drift velocity and diffusion coefficient) and at high ones (ionization coefficient). Moreover, this model can readily be implemented in a device simulator with maximum saving of computation time. The calculations are carried out by employing a standard Monte Carlo simulation, widely used for the study of charge transport in semiconductors [1, 4].

2. Model used

2.1. Monte Carlo simulation

The Monte Carlo algorithm employed in the present study is a three-dimensional simulation of the movement of a single carrier, similar to that described in other works [4, 5]. The semiconductor considered, homogeneous N-type Si, is assumed to be infinite in the three dimensions of space, or at least sufficiently large, and is subject to the action of a constant electric field. The stationary magnitudes are calculated by time-averaging the values obtained from the simulation of the carrier movement over a sufficiently long period of time. If it becomes necessary to obtain information from several carriers, for example to determine the diffusion coefficient [4], an arithmetical mean of the values calculated for each of them is made.

The scattering mechanisms considered in the simulation are the following: intravalley acoustic, intervalley (equivalent and non-equivalent) and interaction with ionized impurities. Acoustic intravalley scattering has been considered to be elastic. The scattering probabilities of the different mechanisms are consistent with the analytical model adopted for the energy bands [4]. The density of donor impurities considered is sufficiently low (10^{13} cm^{-3}) for carrier–carrier scattering to be negligible.

2.2. Band structure and physical parameters

As do other authors [6, 7], we consider for Si a conduction band formed of six equivalent valleys around the six minima of the band along the ⟨100⟩ directions (X valleys) and eight equivalent valleys with the energy minimum in the ⟨111⟩ directions (L valleys). Between the minima of these two types of valleys there is an energy gap of 1.05 eV.

All the valleys are considered to be non-parabolic ellipsoidal. Thus, in a system of axes suitable for each

0268-1242/93/071291 + 07 $07.50

valley, the ε-k relation can be written as:

$$\varepsilon(1 + \alpha_i\varepsilon) = \frac{\hbar^2}{2}\left(\frac{k_l^2}{m_{l_i}^*} + \frac{k_t^2}{m_{t_i}^*}\right) \quad (1)$$

where $\hbar$ is the Planck constant divided by 2π, α_i is the non-parabolicity coefficient of the ith valley, $m_{l_i}^*$ and $m_{t_i}^*$ are the longitudinal and transverse components of the effective mass at the bottom of the ith valley, k_l and k_t are the longitudinal and transverse components of the wavevector, and ε is the kinetic energy of the carrier.

Table 1 shows the Si physical parameters used in the simulation. Those corresponding to the X valleys are similar to those used and accepted by many other authors [7]. Six types of X-X intervalley-phonon scattering are considered, three of f-type (scattering of electrons to any of the four neighbouring valleys) and three of g-type (scattering of electrons to opposite valleys); and four types of X-L intervalley scattering are taken into account. More details about them can be found in [8]. The parameters of the L valleys correspond to those proposed by Fischetti [6]. Although some authors consider the L valleys in their works, they do not include the L-L equivalent intervalley scattering. Consideration of this scattering mechanism will modify the population of these valleys, favouring their importance in transport processes at high electric fields. While for low fields the L valleys have no effect, at high fields, when impact ionization processes occur, they are crucial in the determination of the ionization coefficient.

Owing to the different longitudinal and transverse components of the effective mass of each of the valleys taken into consideration, it is to be expected that certain anisotropies will appear in quantities such as average drift velocity, ionization coefficient etc.

2.3. Impact ionization model

The characterization of the impact ionization processes in Si employing Monte Carlo simulations has been the object of study by many authors, both in semiconductor materials and devices [1, 3, 6, 7, 9]. In general, a complex band structure obtained by the local pseudopotential method is used. The ionization process is usually treated as an additional scattering mechanism whose probability is given by the Keldysh formula [10], with different values of threshold energy, in some cases dependent upon the direction of the wavevector. In contrast to these sophisticated approaches we intend to perform a charac-

Table 1. Si parameters used in the simulation.

Density (g cm^{-3})	2.329	
Sound velocity (10^5 cm s^{-1}):		
transverse	5.30	
longitudinal	9.04	
Dielectric constant	11.70	
Ionized impurity concentration (cm^{-3})	10^{13}	
	X valleys	L valleys
Effective mass (m^*/m_o)		
transverse	0.18	0.126
longitudinal	0.90	1.634
Non-parabolicity (eV^{-1})	0.5	0.5
Energy separation (eV) (relative to X valley)	0	1.05
Number of equivalent valleys	6	8
Acoustic deformation potential (eV)	9	9

Phonon scattering type	Coupling constant (10^8 eV cm^{-1})	Phonon energy (meV)
X–X intervalley scattering		
f_1	0.15	18.1
f_2	3.4	43.1
f_3	4.0	54.3
g_1	0.5	12.1
g_2	0.8	18.1
g_3	3.0	60.3
X–L, L–X intervalley scattering	4.0	57.9
	4.0	54.6
	4.0	41.4
	4.0	17.0
L–L intervalley scattering	2.63	38.87

terization of the ionization processes in Si with a simpler model which fits satisfactorily the available experimental results and can be easily implemented in a device simulator requiring very little computation time.

The model that we develop to obtain both the ionization coefficient and the ionization probability of electrons has already been successfully applied to other semiconductor materials [5, 11]. After completing a free flight, if the electron has a kinetic energy higher than the ionization threshold and the scattering mechanism chosen is an intervalley, impact ionization initiated by that electron occurs. If the scattering mechanism chosen is an interaction with ionized impurities or intravalley acoustic, then the ionization process does not take place, since with these mechanisms it is not possible to assume conservation of momentum in the ionization process.

The threshold energy that we adopt in our model is 2.55 eV, regardless of the direction of the electron wavevector and of the type of valley in which the impact ionization process takes place. This value lies within the range reported for it in Si by Sano *et al* [12]. When an ionization process occurs, this threshold energy is subtracted from the energy of the ionizing electron, and this is its new value at the beginning of the next free flight. In this way energy conservation in the ionization process is ensured.

The model we propose is not hard, since the ionization process does not occur exactly at the time when the carrier attains the threshold energy, but rather when the carrier ends the free flight in which this threshold is surpassed. This affords the model a soft nature, in agreement with the results of Sano *et al* [12].

If during the simulation we record the number of ionization mechanisms taken place in the X and L valleys, N_X and N_L, respectively, and we determine the distance travelled by the electron in the direction of the applied field, D, the ionization coefficient of electrons, α_n, can be obtained as

$$\alpha_n = \frac{N_X + N_L}{D}. \tag{2}$$

Also, the simulation provides the ionization probability given by our model, W_i, through the number of ionization mechanisms and the simulation time, T, as

$$W_i = \frac{N_X + N_L}{T}. \tag{3}$$

The present model constitutes not only a numerical approach for the impact ionization coefficient, but also a consistent method for the study of avalanche multiplication in semiconductor devices. In fact, the approach based on a drift-diffusion model and a field-dependent impact ionization coefficient [13] could not be valid, because the latter and the local field are coupled through the local carrier concentration. Furthermore, our simulation does not need an additional scattering mechanism and/or a complex band structure description for studying the ionization processes. As a consequence of that, it is a suitable model for Monte Carlo device simulation.

3. Results

For each electric field the simulation was performed during 4×10^7 scattering mechanisms. This number is sufficiently high that at low electric fields a suitable distribution of the time spent by the carrier in each of the six X equivalent valleys is achieved, and that at high electric fields the number of ionization processes that take place is sufficient for the results relating to ionization to have statistical validity.

The simulation was carried out for the electric field applied in the ⟨100⟩ and ⟨111⟩ directions, and at a temperature of 300 K.

3.1. Low fields

In order to check the validity of the model at low fields, figure 1 shows the average drift velocity obtained in the simulation with and without considering the interaction with ionized impurities. The drift velocity obtained without ionized impurities ($N_D = 0$) is slightly higher than the experimental values [8], whereas for a density of ionized impurities of $N_D = 10^{13}$ cm^{-3} it is slightly lower. In both cases, as in the experimental results, a slight anisotropy is seen according to the direction of the electric field. The experimental results were obtained in samples made of high-resistivity and high-purity N-type silicon, with $N_D = 5 \times 10^{12}$ cm^{-3}.

Figure 2 reports the results obtained for the mean kinetic energy. For weak fields its value is about 0.039 eV ($\simeq 3/2\, k_B T$), and increases strongly for fields higher than 10 kV cm^{-1}. This increase is less pronounced above 100 kV cm^{-1}, when the carriers begin to pass to the higher valleys (figure 3), losing part of the kinetic energy that they had in the X valleys, which is transformed into potential energy in the L valleys.

Figure 3 shows the fraction of time that the electron remains in each valley. When the electric field is applied in the ⟨111⟩ direction (figure 3(*b*)) the six equivalent X valleys are equally populated, and the L valleys begin to

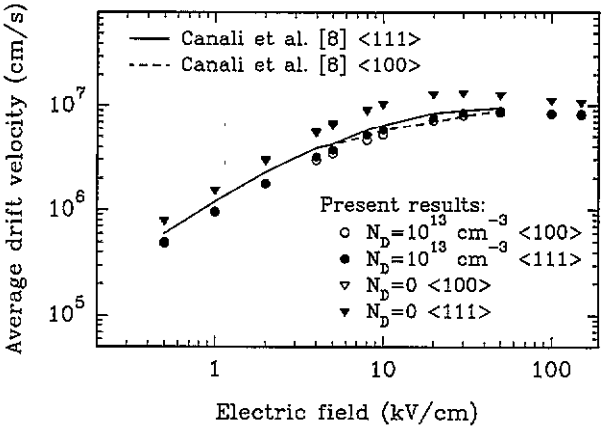

Figure 1. Average drift velocity as a function of electric field between 0 and 100 kV cm^{-1} along the ⟨100⟩ and ⟨111⟩ crystallographic directions. The experimental results are taken from [8].

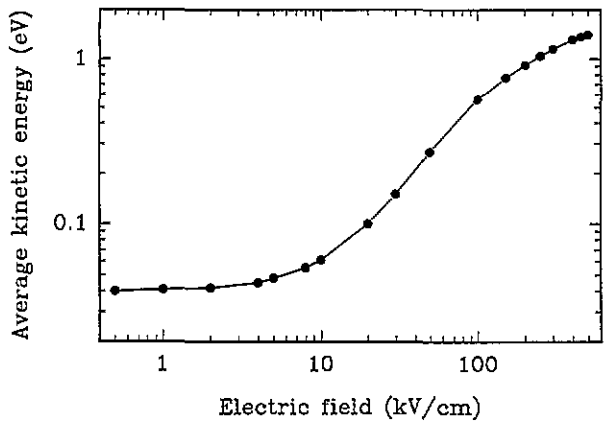

Figure 2. Average kinetic energy as a function of electric field between 0 and 500 kV cm^{-1}. No appreciable differences were observed between the two directions of the electric field applied, and so only one curve is plotted.

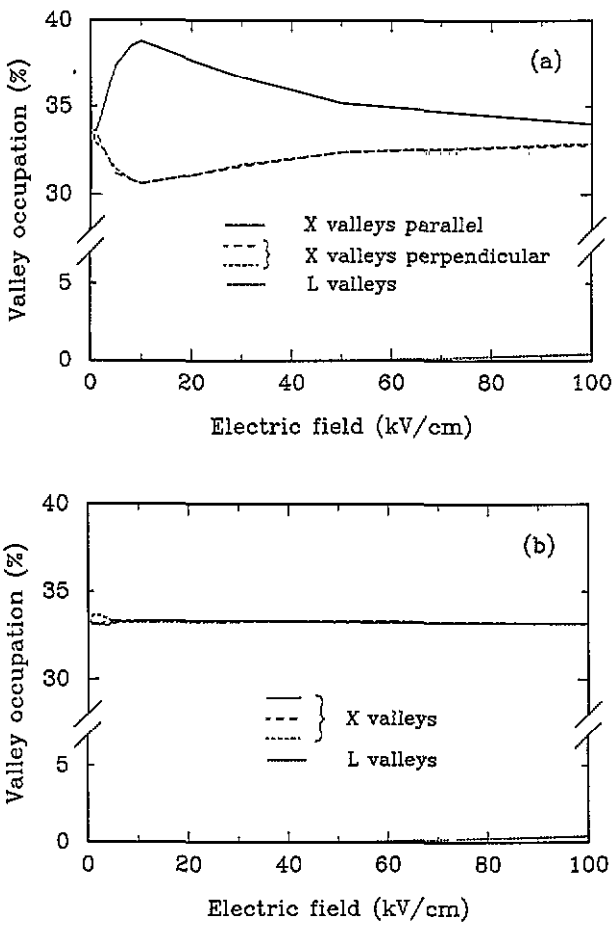

Figure 3. *Fraction of time the electron remains in each* valley as a function of electric field between 0 and 100 kV cm^{-1}. The curve for the L valleys represents the total occupation of the eight L valleys. (*a*) Electric field applied in the ⟨100⟩ direction. (*b*) Electric field applied in the ⟨111⟩ direction.

become significantly occupied for an electric field of 100 kV cm^{-1}. At low electric fields in the ⟨100⟩ direction (figure 3(*a*)) there is a greater population of the X valleys parallel to the electric field. Since the longitudinal component of the effective mass in these valleys is much greater than the transverse one, the carrier gains less energy in them, and the probability of undergoing an equivalent intervalley scattering is smaller than in the perpendicular valleys. This makes the carrier remain longer in the parallel valleys. This difference in the occupation of the X valleys is the origin of the anisotropy observed in the average drift velocity (figure 1). Thus, the velocity is smaller when the field is applied in the ⟨100⟩ direction, since the carrier remains longer in the valleys with a higher effective mass parallel to the field. This anisotropy is stronger for the fields in which the difference between the occupation of the different X valleys is more pronounced.

The values of the longitudinal diffusion coefficient obtained in the simulation for low electric fields are shown in figure 4 together with the available experimental results [14]. These values have been calculated from the slope of the second central moment of an ensemble of carriers [4], and have been found to be very sensitive to the impurity concentration. The good agreement with the experimental data found for this magnitude constitutes a verification of the validity of the method and the physical parameters adopted.

3.2. High fields

Figure 5 shows the drift velocity as a function of electric field between 100 and 500 kV cm^{-1}. A slight negative differential mobility appears around 150 kV cm^{-1}, which is consistent with the results of previous Monte Carlo simulations [7], and it is due to the onset of the X-L intervalley scattering. For this field range no differences between the results for the ⟨100⟩ and ⟨111⟩ field directions are detected, owing to the high efficiency of the intervalley mechanisms.

The valley occupation for the 100–500 kV cm^{-1} electric field range is shown in figure 6. The difference between the population of the different X valleys that was observed for low fields in the ⟨100⟩ direction (figure 3(*a*))

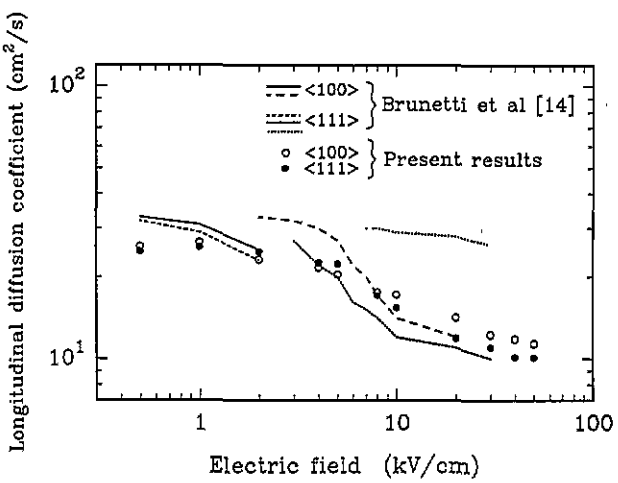

Figure 4. Longitudinal diffusion coefficient as a function of electric field in the ⟨100⟩ and ⟨111⟩ directions. The experimental results are taken from [14].

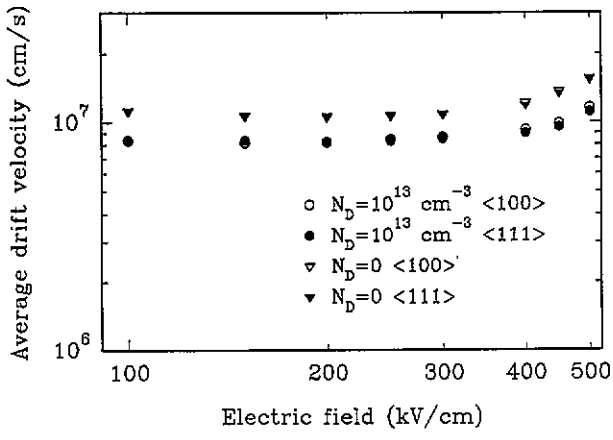

Figure 5. Average drift velocity as a function of electric field between 100 and 500 kV cm^{-1} in the ⟨100⟩ and ⟨111⟩ crystallographic directions.

is now very small (figure 6(*a*)), because of the action of the intervalley mechanisms. As the field increases, the occupation of the L valleys becomes increasingly important, reaching a value of about 11% for 500 kV cm^{-1}. Above this field the valley population becomes stabilized. These results imply that the L valleys will play an important role in the transport processes in Si at very high fields.

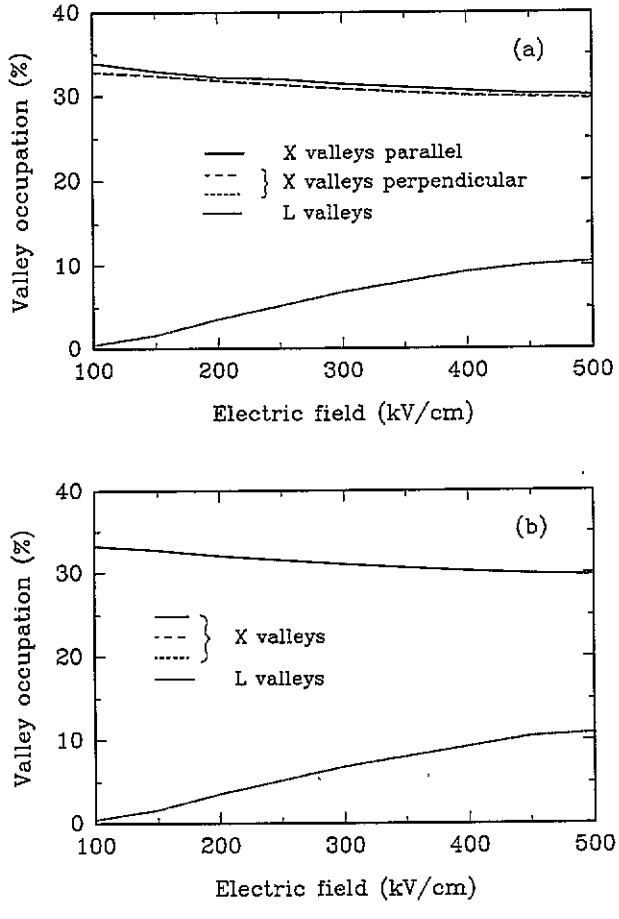

Figure 6. Fraction of time the electron remains in each valley as a function of electric field between 100 and 500 kV cm^{-1}. The line for the L valleys represents the total occupation of the eight L valleys. (a) Electric field applied in the ⟨100⟩ direction. (*b*) Electric field applied in the ⟨111⟩ direction.

Figure 7 shows the ionization coefficient of electrons in Si (equation (2)) together with several experimental values [15–17]. Within the 200–500 kV cm^{-1} electric field range the values obtained are consistent with the experimental ones. For lower electric fields we are not aware of any experimental results, and those of our simulation are in agreement with those reported by Fischetti [6], also calculated from Monte Carlo simulations. Whereas for fields between 50 and 150 kV cm^{-1} the ionization coefficient is slightly higher in the ⟨111⟩ direction, for higher fields (150–500 kV cm^{-1}) it is larger in the ⟨100⟩ direction. This is logical taking into account the values of the longitudinal and transverse components of the effective masses of the X and L valleys. The population of the L valleys, with their revolution axes in the ⟨111⟩ directions and a greater longitudinal mass, begins to become significant for fields higher than 150 kV cm^{-1}. This means that for very high fields in the ⟨111⟩ direction it is a more difficult for the carrier to gain energy in the L valleys than when the field is applied in the ⟨100⟩ direction, and therefore the number of ionization processes taking place is lower. This effect shows the importance of the L valleys in high-field transport phenomena.

Figure 8 shows the ionization coefficient of electrons for two different ranges of the electric field (higher than 500 kV cm^{-1}, and between 50 and 125 kV cm^{-1}), where it has been found to follow a dependence on the field of the form

$$\alpha_n = A \exp[-(B/E)^n] \qquad (4)$$

for $n = 1$ and with different constants A and B in each of these two ranges, whose values are given in table 2. This type of dependence corresponds to the general expression proposed by Baraff [18], where the coefficients A and B depend on the effective mass of the energy bands considered, and it is usually employed for including the ionization processes in drift-diffusion models [13]. In the

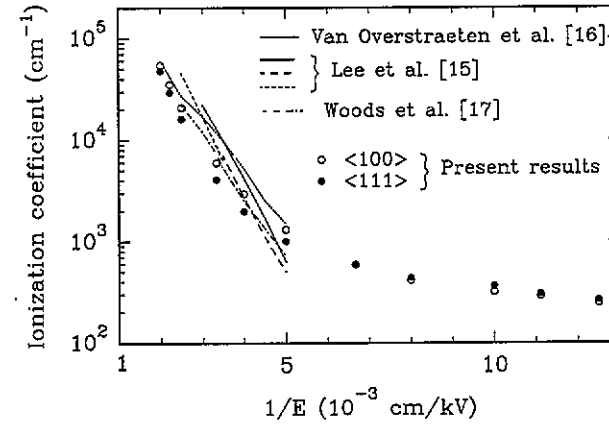

Figure 7. Calculated electron impact ionization coefficient as a function of inverse electric field along the ⟨100⟩ and ⟨111⟩ crystallographic directions. The experimental results are taken from [15–17].

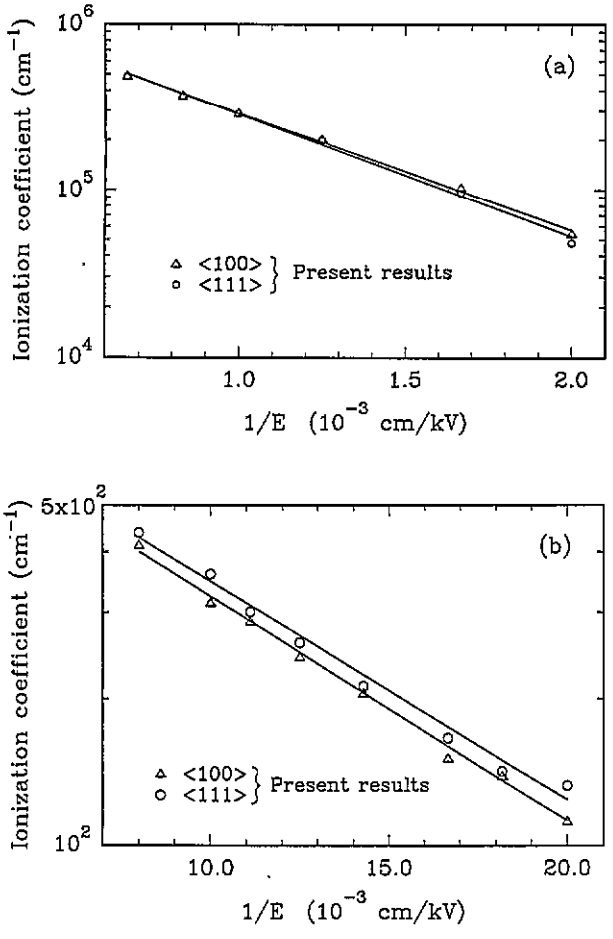

Figure 8. Ionization coefficient of electrons as a function of inverse electric field in the ⟨100⟩ and ⟨111⟩ crystallographic directions. (*a*) For fields higher than 500 kV cm^{-1}. (*b*) Between 50 and 125 kV cm^{-1}. The lines correspond to equation (4) with $n = 1$ and the values given in table 2 for the constants *A* and *B*.

Table 2. Values for the constants *A* and *B* of equation (4) to fit the ionization coefficient of electrons for two electric field ranges in the ⟨100⟩ and ⟨111⟩ directions.

Field range (kV cm^{-1})	Direction	*A* (cm^{-1})	*B* (kV cm^{-1})
50–125	⟨100⟩	9.36×10^2	1.06×10^2
	⟨111⟩	9.75×10^2	1.03×10^2
500–2000	⟨100⟩	1.49×10^6	1.63×10^3
	⟨111⟩	1.57×10^6	1.70×10^3

150–500 kV cm^{-1} electric field range this relation does not hold, since the population of the L valleys is not stabilized (figure 6), and therefore the constants are expected to depend on the field through the combined contribution of the L and X valleys.

Figure 9 shows the ionization probability obtained from equation (3) as a function of the average kinetic energy, together with that reported by other authors [3, 19]. They adopt the Keldysh empirical formula [10] to represent the ionization probability, with different values

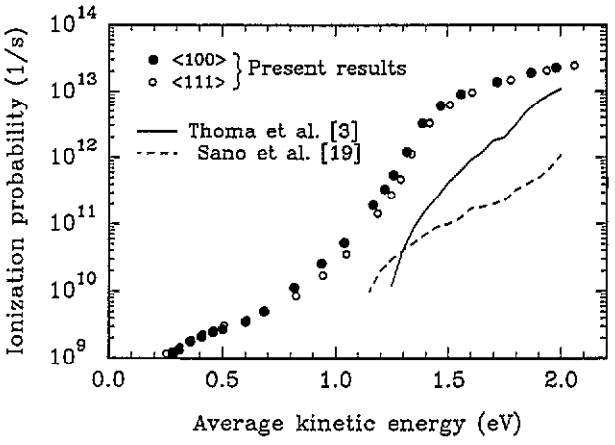

Figure 9. Calculated ionization probability as a function of the average kinetic energy, and theoretical values reported in [3, 19].

of threshold energy. The ionization probability given by our model, having the same shape, is found to be higher than that of those authors. This can be partially attributed to the fact that their ionization probability is given versus the total energy of the carrier, while we consider the kinetic energy, and when the L valleys become populated there is an important difference between the two energies.

4. Conclusions

We have presented a Monte Carlo analysis of electron transport in Si for both low and high electric fields, employing a model for the conduction band formed of non-parabolic ellipsoidal X and L valleys. One of the novelties introduced in the present simulation is the consideration of L–L intervalley scattering mechanisms, which makes these valleys more important in transport processes at high fields. The results for low fields (drift velocity, diffusion coefficient) are in accordance with the available experimental results, thus supporting the validity of the model.

Several results depend on the electric field direction (drift velocity, ionization coefficient). This anisotropy has been explained in terms of the different longitudinal and transverse components of the effective mass of the valleys and their occupation.

A simple model for the characterization of the impact ionization processes has been proposed and tested in the simulations, giving favourable results. The ionization coefficients obtained are consistent with the experimental results, and the ionization probability provided by our model is found to be analogous to that reported by other authors who assume for it an analytical expression.

Acknowledgments

This work has been funded through an agreement with IBM SAE, and the Special Action TIC92-0229-E from the CICYT.

References

[1] Fischetti M and Laux S 1988 *Phys. Rev.* B **38** 9721
[2] Brunetti R, Jacoboni C, Venturi F, Sangiorgi E and Ricco B 1989 *Solid-State Electron.* **32** 1663
[3] Thoma R, Peifer H and Engl W 1991 *J. Appl. Phys.* **69** 2300
[4] Jacoboni C and Reggiani L 1989 *The Monte Carlo Method for Semiconductor Device Simulation* (Vienna: Springer)
[5] González T, Velázquez J, Gutierrez P and Pardo D 1991 *Semicond. Sci. Technol.* **6** 862
[6] Fischetti M 1991 *IEEE Trans. Electron Devices* **38** 634
[7] Sano N, Aoki T, Tomizawa M and Yoshii A 1990 *Phys. Rev.* B **41** 12122
[8] Canali C, Jacoboni C, Nava F, Ottaviani G and Alberigi-Quaranta A 1975 *Phys. Rev.* B **12** 2265
[9] Tang J and Hess K 1983 *J. Appl. Phys.* **54** 5139
[10] Keldysh V 1965 *Sov. Phys.–JETP* **21** 1135
[11] González T, Velázquez J, Gutierrez P and Pardo D 1992 *Semicond. Sci. Technol.* **7** 31
[12] Sano N, Aoki T and Yoshii A 1989 *Appl. Phys. Lett.* **55** 1418
[13] Wada Y and Tomizawa M 1988 *IEEE Trans. Electron Devices* **35** 1765
[14] Brunetti R, Jacoboni C, Nava F, Reggiani L, Bosman G and Zijlstra A 1981 *J. Appl. Phys.* **52** 6713
[15] Lee C, Logan R, Batdorf R, Kleimack J and Wiegmann W 1964 *Phys. Rev.* **134** A761
[16] Van Overstraeten R and De Man H 1970 *Solid-State Electron.* **13** 583
[17] Woods M, Johnson W and Lampert M 1973 *Solid-State Electron.* **16** 381
[18] Baraff G 1962 *Phys. Rev.* **128** 2507
[19] Sano N, Tomizawa M and Yoshii A 1991 *Japan. J. Appl. Phys.* **30** 3662